ACS APPLIED MATERIALS & INTERFACES

Research Article

www.acsami.org

Ruthenium(0) Nanoparticles Supported on Multiwalled Carbon Nanotube As Highly Active Catalyst for Hydrogen Generation from Ammonia–Borane

Serdar Akbayrak and Saim Özkar*

Department of Chemistry, Middle East Technical University, 06800, Ankara, Turkey

Supporting Information

ABSTRACT: Ruthenium(0) nanoparticles supported on multiwalled carbon nanotubes (Ru(0)@MWCNT) were in situ formed during the hydrolysis of ammonia–borane (AB) and could be isolated from the reaction solution by filtration and characterized by ICP-OES, XRD, TEM, SEM, EDX, and XPS techniques. The results reveal that ruthenium(0) nanoparticles of size in the range 1.4–3.0 nm are well-dispersed on multiwalled carbon nanotubes. They were found to be highly active catalyst in hydrogen generation from the hydrolysis of AB with a turnover frequency value of 329 min^{-1}. The reusability experiments show that Ru(0)@MWCNTs are isolable and redispersible in aqueous solution; when redispersed they are still active catalyst in the hydrolysis of AB exhibiting a release of 3.0 equivalents of H_2 per mole of NH_3BH_3 and preserving 41% of the initial catalytic activity even after the fourth run of hydrolysis. The lifetime of Ru(0)@MWCNTs was measured as 26400 turnovers over 29 h in the hydrolysis of AB at 25.0 ± 0.1 °C before deactivation. The work reported here also includes the kinetic studies depending on the temperature to determine the activation energy of the reaction (E_a = 33 ± 2 kJ/mol) and the effect of catalyst concentration on the rate of the catalytic hydrolysis of AB, respectively.

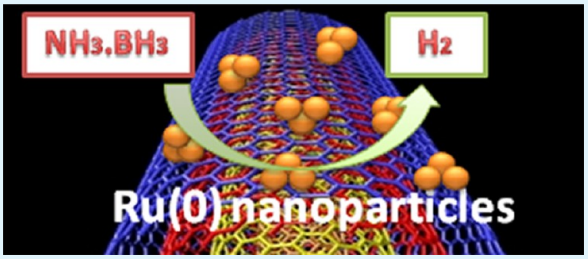

KEYWORDS: *ruthenium nanoparticles, carbon nanotube, heterogeneous catalyst, hydrogen generation, ammonia borane, hydrolysis*

INTRODUCTION

Secure storage and effective release of hydrogen are very important in the application of hydrogen energy.[1,2] Tremendous efforts have been devoted to research and development on materials that can hold sufficient hydrogen in terms of gravimetric and volumetric densities and have suitable thermodynamic and kinetic properties.[3] Long-term exploration has shown that the most effective and safest way of storing hydrogen is to use solid media such as sorbent materials[4,5] or hydrides.[6−8] Among the chemical hydrides, ammonia–borane ($H_3N{\cdot}BH_3$, AB) appears to be an appropriate hydrogen storage materials because of its high hydrogen content of 19.6 wt %, high stability under ambient conditions, and nontoxicity.[9−11] Hydrogen stored in the AB complex can be released by either thermal dehydrogenation[12] or solvolysis.[13] Because the dehydrogenation temperature is relatively high[14] (greater than 100 °C), there has been enormous interest on the catalytic methanolysis[15−17] and hydrolysis of AB (eq 1) using transition metal catalysts including platinum,[18] ruthenium,[19,20] rhodium,[21−23] palladium,[24,25] iron,[26] cobalt,[27−31] and nickel.[32,33]

$$H_3NBH_3(aq) + 2H_2O(l) \xrightarrow{\text{catalyst}} NH_4^+(aq) + BO_2^-(aq) + 3H_2(g) \quad (1)$$

However, most of these transition metal catalysts are in the form of nanoparticles that suffer in long-term stability because of the aggregation into clumps and ultimately to the bulk metal, despite using the best stabilizers,[34,35] which leads to a decrease in catalytic activity and lifetime. The use of nanoclusters catalysts in systems with confined void spaces such as zeolite has been shown to be an efficient way of preventing aggregation.[22,24,25,29] Despite the high activity and long lifetime of the zeolite confined metal(0) nanoclusters catalysts, they have two major drawbacks: diffusion controlled kinetics and migration of metal to the external surface at high temperature. With high external surface area and aspect ratio,[36,37] carbon nanotubes appear to be very attractive as catalyst supports in liquid phase reactions as they provide high dispersion of nanoparticles, significantly increase contact surface between the reactants and active sites, and greatly minimize the diffusion limitations, compared with traditional catalyst supports.[38−41] Among the reported studies, there exists various examples of carbon-nanotube-supported ruthenium catalysts formed by using additional reducing agents such as H_2(g) at high temperature[36,40] or ethylene glycol,[37] or formed after impregnation of ruthenium on carbon nanotubes with a high Ru/C ratio of 1:1 at high temperature.[41] Such a high-temperature treatment might cause alteration in the catalyst

Received: September 7, 2012
Accepted: November 1, 2012
Published: November 1, 2012

 © 2012 American Chemical Society dx.doi.org/10.1021/am3019146 | ACS Appl. Mater. Interfaces 2012, 4, 6302–6310

materials and high ruthenium loading results in the formation of large nanoparticles. Herein, we report the in situ generation of ruthenium(0) nanoparticles supported on multiwalled carbon nanotubes (MWCNT) catalyst during the hydrolysis of AB at room temperature. Ruthenium(III) ions were impregnated on the surface of MWCNT from the aqueous solution of ruthenium(III) chloride and then reduced by ammonia–borane forming the ruthenium(0) nanoparticles supported on multiwalled carbon nanotubes, hereafter referred to as Ru(0)@MWCNT, which were isolated from the reaction solution by filtration and characterized by ICP-OES, XRD, SEM, EDX, TEM, and XPS techniques. All the results reveal that ruthenium nanoparticles of size in the rage 2.0–3.0 nm are well-dispersed on the wall of carbon nanotubes and have remarkable catalytic activity in the hydrolysis of AB with a turnover frequency of 329 min^{-1} at 25 ± 0.1 °C. The reusability and catalytic lifetime experiments also indicate that Ru(0)@MWCNT is an efficient, reusable, and long-lived catalyst in the hydrolysis of AB releasing 3.0 equiv. of H_2 per NH_3BH_3 present in the solution.

EXPERIMENTAL SECTION

Materials. Ruthenium(III) chloride trihydrate ($RuCl_3{\cdot}3H_2O$) and ammonia–borane (AB, 97%) were purchased from Aldrich. Multiwalled carbon nanotubes (MWCNTs) with a diameter of 150 nm were purchased from Electrovac, Kalosterneuburg, Austria. Deionized water was distilled by water purification system (Milli-Q System).

Characterization. The ruthenium contents of the Ru(0)@MWCNT samples were determined by inductively coupled plasma optical emission spectroscopy (ICP-OES, Leeman-Direct Reading Echelle) after each sample was completely dissolved in the mixture of HNO_3/HCl (1/3 ratio). Transmission electron microscopy (TEM) was performed on a JEM-2100F (JEOL) microscope operating at 200 kV. A small amount of powder sample was placed on the holey carbon grid of the transmission electron microscope. Samples were examined at magnification between 100 and 400 K. Scanning electron microscope (SEM) images were taken using a JEOL JSM-5310LV at 15 kV and 33 Pa in a low-vacuum mode without metal coating on aluminum support. The X-ray photoelectron spectroscopy (XPS) analysis was performed on a Physical Electronics 5800 spectrometer equipped with a hemispherical analyzer and using monochromatic Al Kα radiation of 1486.6 eV, the X-ray tube working at 15 kV, 350 W, and pass energy of 23.5 keV. The sample surface was sputtered by argon ion bombardment with 2000 eV energy for 3 min. ^{11}B NMR spectra were recorded on a Bruker Avance DPX 400 with an operating frequency of 128.15 MHz for ^{11}B.

Impregnation of Ruthenium(III) Ions on Multiwalled Carbon Nanotubes (Ru(III)@MWCNT). Multiwalled carbon nanotubes were refluxed in a mixture of HNO_3 (36 mL)/H_2SO_4 (54 mL) at 80 °C for 6 h. The mixture was then filtered and washed with distilled water until the pH value of filtrate reached 7. The functionalized multiwalled carbon nanotubes were dried at 120 °C for 12 h in the oven. The dried MWCNTs (100 mg) were stirred in 100 mL of an aqueous solution of 6.56 mg of $RuCl_3{\cdot}3H_2O$ for 72 h at room temperature. The sample was then filtered using a funnel with sintered glass filter and washed with 100 mL of distilled water and the remnant was dried at 120 °C for 12 h in the oven.

In situ Formation of Ruthenium(0) Nanoparticles Supported on Multiwalled Carbon Nanotubes (Ru(0)@MWCNT) and Concomitant Catalytic Hydrolysis of Ammonia–Borane. Ruthenium(0) nanoparticles supported on multiwalled carbon nanotubes were in situ generated from the reduction of Ru(III)@MWCNT during the catalytic hydrolysis of AB. Before starting the catalyst formation and concomitant catalytic hydrolysis of AB, a jacketed reaction flask (20 mL) containing a Teflon-coated stir bar was placed on a magnetic stirrer (Heidolph MR-301) and thermostatted to 25.0 ± 0.1 °C by circulating water through its jacket from a constant temperature bath. Then, a graduated glass tube (60 cm in height and 3.0 cm in diameter) filled with water was connected to the reaction flask to measure the volume of the hydrogen gas to be evolved from the reaction. Next, 10 mg powder of Ru(III)@MWCNT (1.91 wt % Ru) was dispersed in 10 mL of distilled water in the reaction flask thermostatted at 25.0 ± 0.1 °C. Then, 31.8 mg of AB (1.0 mmol $H_3N.BH_3$) was added into the flask and the reaction medium was stirred at 1000 rpm. After a short induction period of less than 1.0 min, ruthenium(0) nanoparticles were formed and the catalytic hydrolysis of AB started. The volume of hydrogen gas evolved was measured by recording the displacement of water level every 30 s at constant atmospheric pressure of 693 Torr. The reaction was stopped when no more hydrogen evolution was observed. In each experiment, the resulting solutions were filtered and the filtrates were analyzed by ^{11}B NMR and conversion of AB to metaborate anion was confirmed by comparing the intensity of signals in the ^{11}B NMR spectra of the filtrates.

Determination of the Most Active Ruthenium Loading for Ru(0)@MWCNT Used in the Hydrolysis of AB. The catalytic activity of Ru(0)@MWCNT samples with various ruthenium loading in the range of 0.7–2.8 wt % was tested in hydrogen generation from the hydrolysis of AB starting with 0.216 mM Ru and 100 mM AB in 10 mL solution at 25 ± 0.1 °C.The highest catalytic activity was achieved by using 1.91 wt % ruthenium-loaded multiwalled carbon nanotubes. For all the tests reported hereafter, ruthenium loading of 1.91 wt % was used unless otherwise stated.

Determination of Activation Energy for Hydrolysis of AB Catalyzed by Ru(0)@MWCNT. In a typical experiment, the hydrolysis reaction was performed starting with 10 mL of 100 mM (31.8 mg) AB solution and 10 mg of Ru(III)@MWCNT (1.91 wt % ruthenium, [Ru] = 0.189 mM) at various temperatures (20, 25, 30, 35, 40 °C) in order to obtain the activation energy (E_a).

Reusability of Ru(0)@MWCNT in the hydrolysis of AB. After the complete hydrolysis of AB started with 10 mL of 100 mM AB (31.8 mg H_3NBH_3), and 30 mg Ru(III)@MWCNT (1.91 wt % ruthenium, [Ru] = 0.567 mM) at 25 ± 0.1 °C, the catalyst was filtered through a sintered glass funnel and washed with 100 mL water and dried in the oven at 120 °C. The isolated samples of Ru(0)@MWCNTs were weighed and redispersed in 10 mL solution of 100 mM AB for a subsequent run of hydrolysis at 25 ± 0.1 °C.

Determination of the Catalytic Lifetime of Ru(0)@MWCNT in the Hydrolysis of AB. The catalytic lifetime of Ru(0)@MWCNT in the hydrolysis of AB was determined by measuring the total turnover number (TTO). Such a lifetime experiment was started with a 100 mL solution containing 0.0189 mM Ru(III)@MWCNT and 30 mM AB at 25.0 ± 0.1 °C. When all the ammonia–borane present in the solution was completely hydrolyzed, more AB was added and the reaction was continued in this way until no hydrogen gas evolution was observed.

RESULTS AND DISCUSSION

In situ generation, Isolation and Characterization of Ru(0)@MWCNT. Ruthenium(0) nanoparticles supported on multiwalled carbon nanotubes were in situ generated during the hydrolysis of ammonia–borane. Ruthenium(III) ions were impregnated on the acid treated MWCNT from the aqueous solution of ruthenium(III) chloride and then reduced by AB at room temperature. When AB solution is added to the suspension of ruthenium(III) ions impregnated on carbon nanotubes, both reduction of ruthenium(III) to ruthenium(0) and hydrogen release from the hydrolysis of AB occur concomitantly. The progress of ruthenium(0) nanoparticles formation and concomitant dehydrogenation of ammonia–borane was followed by monitoring the changes in H_2 pressure. Figure 1 shows the plot of equivalent H_2 generated versus time for the hydrolysis of AB starting with Ru(III)@MWCNT precatalyst (0.378 mM Ru) and 100 mM AB in 10 mL aqueous solution at 25.0 ± 0.1 °C. After a short induction period of 1.0 min, the hydrogen generation starts and continues almost linearly until the release of 3 equiv. H_2 per equivalent of AB.

dx.doi.org/10.1021/am3019146 | ACS Appl. Mater. Interfaces 2012, 4, 6302–6310

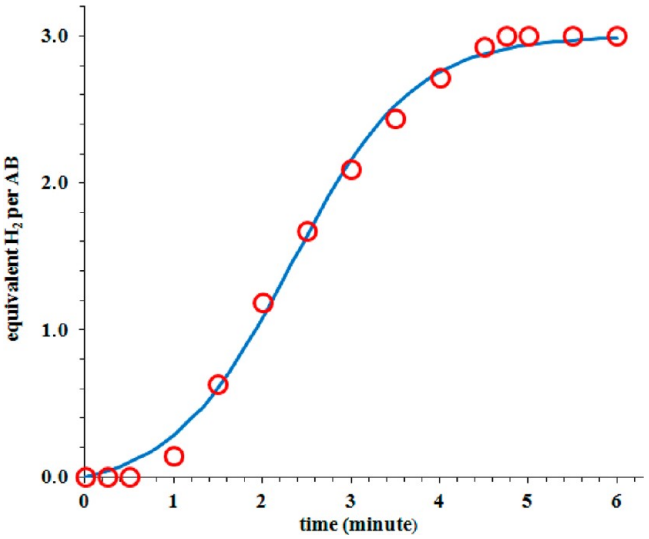

Figure 1. Plot of equivalent H_2 generated versus time for the hydrogen generation from the hydrolysis of ammonia–borane (AB) starting with 20 mg Ru(0)@MWCNT (with a loading of 1.91 wt % Ru) as catalyst and 1.0 mmol AB in 10 mL of aqueous solution at 25.0 ± 0.1 °C. The sigmoidal curve fits well to the two-step mechanism for the ruthenium(0) nanoparticle formation.

The observation of an induction period and a sigmoidal shape of dehydrogenation curve indicates the formation of ruthenium(0) nanoparticles with a two-step, nucleation and autocatalytic growth mechanism.[42,43] The formation kinetics of the $Ru(0)_n$ nanoparticle catalyst can be obtained using the hydrogen release from AB as reporter reaction,[44] given in Scheme 1, in which A is the added precursor Ru(III)@MWCNT and B is the growing $Ru(0)_n$ nanoparticles on the surface of MWCNT. The hydrogen generation from the hydrolysis of AB will accurately report on and amplifies the amount of $Ru(0)_n$ nanoparticle catalyst B present if the dehydrogenation rate is fast in comparison to the rate of nanoparticles formation. It was shown that the dehydrogenation is zero-order in [AB] to ensure that the dehydrogenation reporter reaction is fast relative to the rate of slower nanoparticle formation k_1 and k_2 steps (Scheme 1). Sigmoidal kinetics can be seen in Figure 1 and fit well by the Finke-Watzky two-step, nucleation, and autocatalytic growth mechanism of nanoparticle formation.[42] The observation of a sigmoidal dehydrogenation curve and its curve-fit to the slow, continuous nucleation, A → B (rate constant k_1) followed by autocatalytic surface growth, A + B → 2B (rate constant k_2) kinetics are very strong evidence for the formation of metal(0) nanoparticles catalyst from a soluble transition-metal complex in the presence of reducing agent.[42] The rate constants determined from the nonlinear least-squares curve-fit in Figure 1 are $k_1 = 4.6 \times 10^{-2}$ min^{-1} and $k_2 = 5.0 \times 10^{2}$ M^{-1} min^{-1}. The mathematically required correction has been made to k_2 for the stoichiometry factor of 1058 as described elsewhere,[43] but not for the "scaling factor"; that is no correction has been made for the changing the number of Ru atoms on the growing metal surface.[43]

Scheme 1. Illustration of the Hydrogen Release from the Catalytic Hydrolysis of Ammonia–Borane As Reporter Reaction: A is the Precursor Ru(III)@MWCNT and B is the Growing $Ru(0)_n$ Nanoparticles on the Surface of MWCNTs

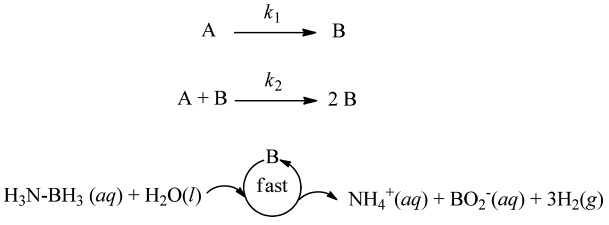

The ruthenium(0) nanoparticles supported on multiwalled carbon nanotubes (Ru(0)@MWCNT), in situ formed during the hydrolysis of AB, could be isolated from the reaction solution as powder by filtration and characterized by ICP-OES, XRD, SEM, EDX, TEM, and XPS techniques. Ruthenium content of Ru(0)@MWCNT was determined by ICP-OES. The XRD patterns of pristine MWCNT, acid-treated MWCNT and Ru(0)@MWCNT are given altogether in Figure 2 for comparison. A comparison of the XRD patterns of pristine MWCNT and acid-treated MWCNT given in panels a and b in Figure 2, respectively, clearly shows that there is no change in the characteristic diffraction peaks of multiwalled carbon nanotubes after acid treatment indicating that MWCNTs were not severely damaged by refluxing in the mixture of HNO_3/H_2SO_4.[45] The diffraction peaks at 26.2, 43.3, and 54.5° could be well-indexed as (002), (100), and (004) reflections of graphite structure, respectively.[46] XRD patterns of acid treated MWCNT (Figure.2b) and Ru(0)@MWCNT with a ruthenium loading of 1.91 wt % Ru (Figure 2c) are almost identical. There is no observable peak attributable to ruthenium nanoparticles in Figure 2c, probably as a result of low ruthenium loading of materials.[47] The BET nitrogen adsorption analysis gave the surface area of acid treated MWCNT and Ru(0)@MWCNT as 41 and 31 m^2 g^{-1}, respectively. Because ruthenium(0) nanoparticles can easily migrate and block the entrance of MWCNT during the thermal treatment at temperatures up to 300 °C under vacuum (1×10^{-3} to 1×10^{-4} Torr) a decrease in the amount of N_2 adsorbed on the walls of MWCNT is expected upon ruthenium loading. Therefore, the noticeable decrease in the surface area of carbon nanotubes upon

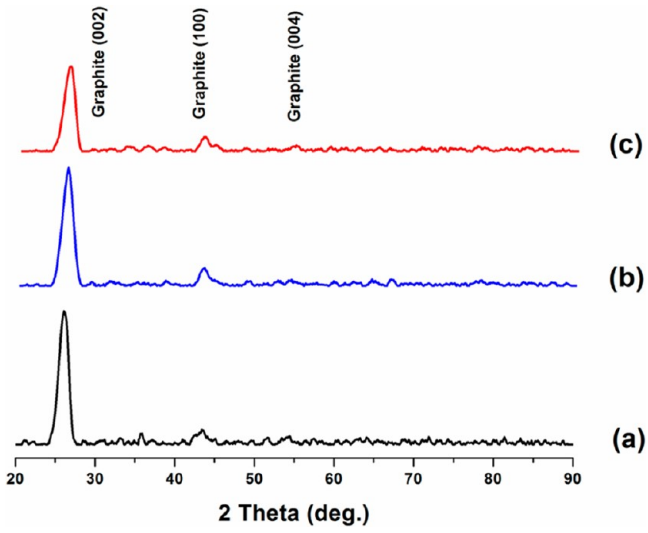

Figure 2. XRD patterns of (a) pristine MWCNT, (b) acid-treated MWCNT, (c) Ru(0)@MWCNT with a 1.91 wt % Ru loading.

dx.doi.org/10.1021/am3019146 | ACS Appl. Mater. Interfaces 2012, 4, 6302–6310

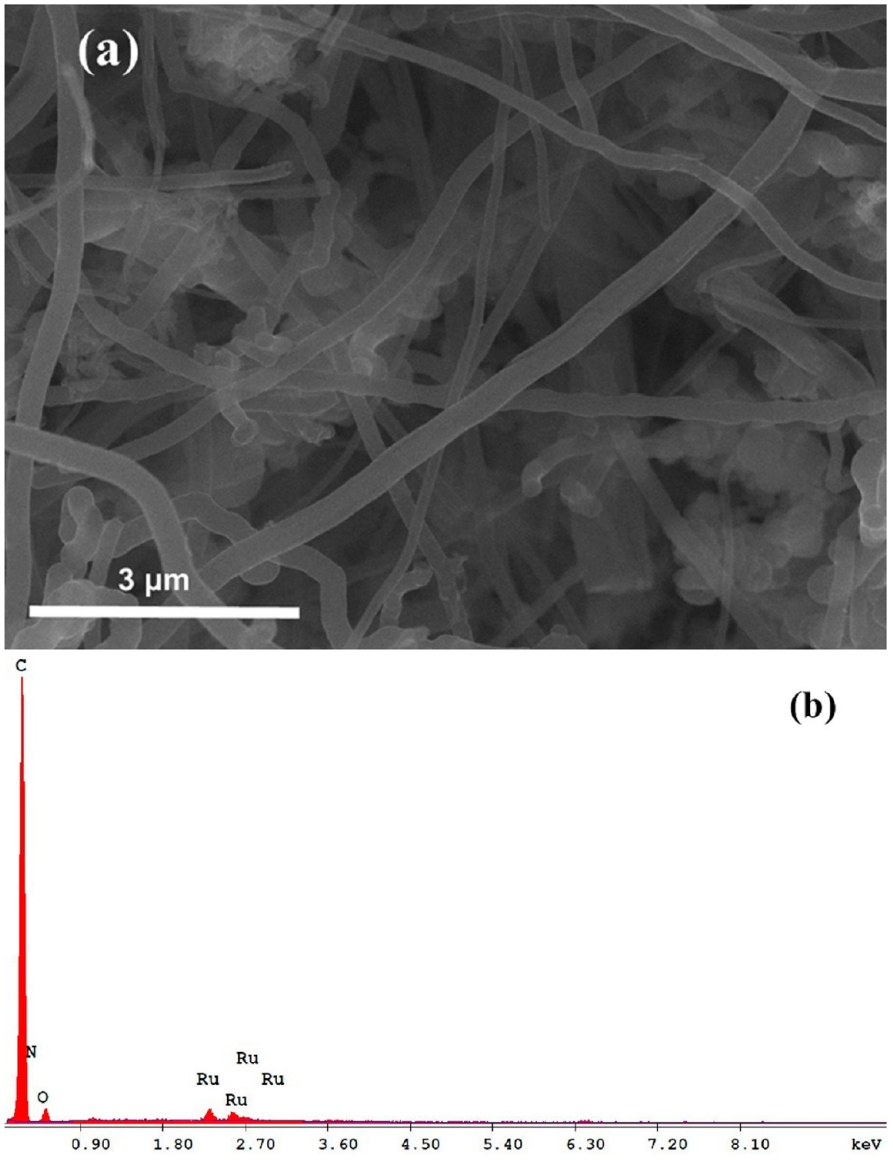

Figure 3. (a) SEM image (The scale bar is 3 μm), (b) SEM-EDX spectrum of Ru(0)@MWCNT with a 1.91 wt % Ru loading.

ruthenium loading implies the existence of ruthenium(0) nanoparticles on the surface.

Figure 3 exhibits the SEM image and SEM-EDX spectrum of Ru(0)@MWCNT with a ruthenium loading of 1.91 wt % indicating that (i) acid treatment caused no damage to the wall of carbon nanotubes in agreement with XRD results and (ii) ruthenium is the only element detected in the sample in addition to the surface elements of carbon nanotubes (N, C, O) because of functional groups formed after acid treatment.

Figure 4 shows the TEM images of acid treated MWCNTs and Ru(0)@MWCNT taken with different magnifications. From the TEM images given in Figures 4b–d, one can see that (i) highly dispersed ruthenium(0) nanoparticles are formed on the surface of MWCNTs with particle size in the range 1.4–3.0 nm (mean diameter: 2.5 ± 0.8 nm, histogram in Figure 4e) and (ii) neither the acid treatment nor the impregnation of ruthenium(III) followed by reduction to ruthenium(0) causes any damage to the wall of carbon nanotubes in agreement with the XRD results.

The composition of Ru(0)@MWCNT formed in situ during the hydrolysis of AB and the oxidation state of ruthenium were also studied by XPS technique. High-resolution X-ray photoelectron spectrum of a Ru(0)@MWCNT sample with metal loading of 1.91 wt % Ru given in Figure 5 shows two prominent bands at 284.4 and 280.2 eV, which can readily be assigned of Ru(0) $3d_{3/2}$ and $3d_{5/2}$, respectively, in the nanoparticles by comparing with values of ruthenium metal 285 and 280 eV, respectively.[48] It is noteworthy that the Ru(0) $3d_{3/2}$ peak at 284.4 eV overlaps with the C 1s peak at 283.9 eV coming from multiwalled carbon nanotubes with a percent atomic ratio of 14.63 (C 1s/Ru 3d).

Catalytic Activity of Ru(0)@MWCNT in the Hydrolysis of AB. Before starting with the investigation on the catalytic activity of Ru(0)@MWCNT in the hydrolysis of AB, a control experiment was performed to check whether the acid treated MWCNTs show any catalytic activity in the hydrolysis of AB at the same temperature. In a control experiment starting with 1.0 mmol of AB and 10 mg of powder of MWCNT (the same amount as the one used in catalytic activity tests) in 10 mL of water at 25.0 ± 0.1 °C or 40.0 ± 0.1 °C, no hydrogen generation was observed in 1 h at both temperatures. This observation indicates that the hydrolysis of AB does not occur

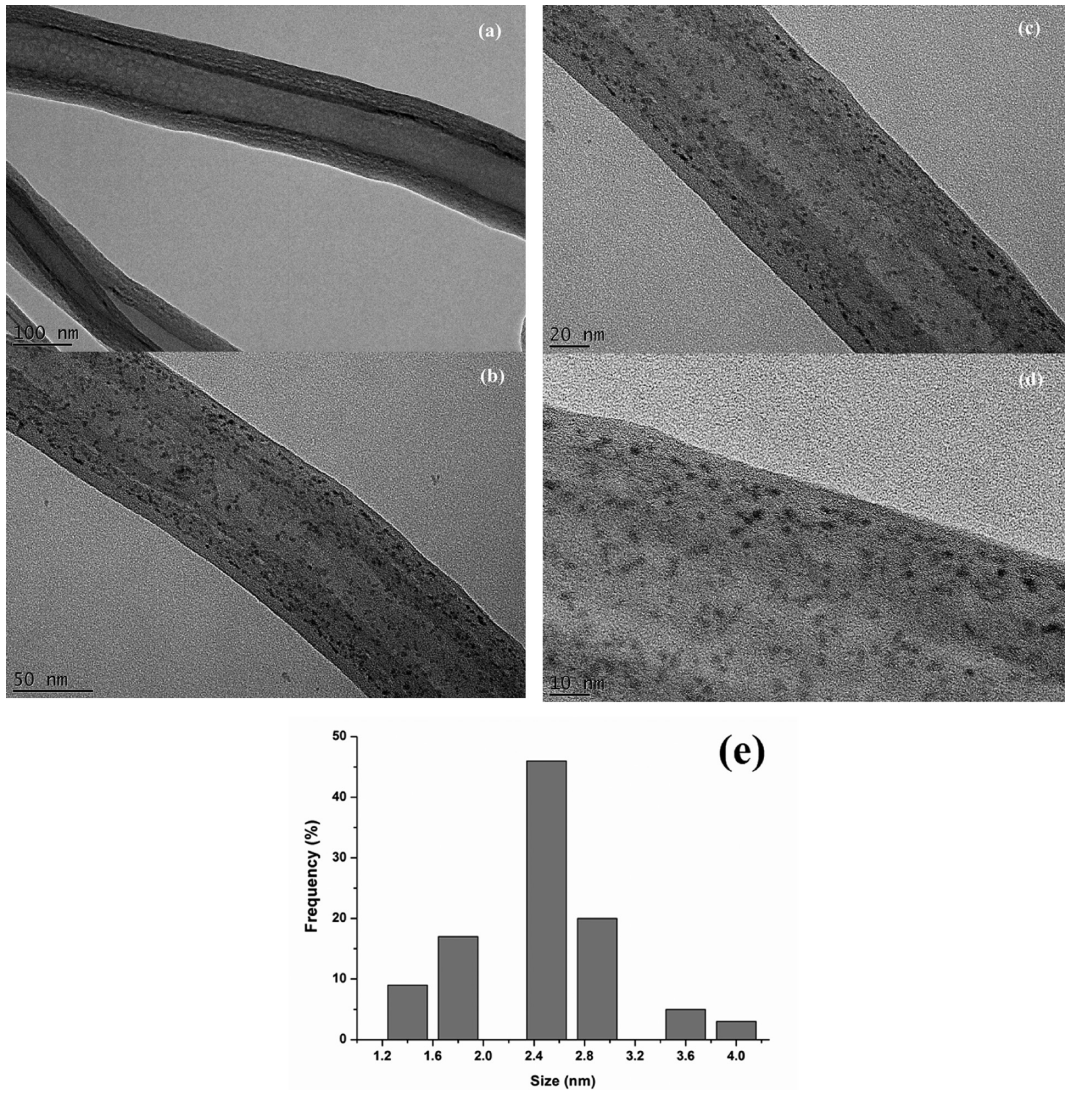

Figure 4. TEM images of (a) the acid-treated MWCNTs (the scale bar is 100 nm) and Ru(0)@MWCNT with a 1.91 wt % Ru loading in different magnifications with scale bars of (b) 50, (c) 20, and (d) 10 nm, and (e) the corresponding histogram for the particle size distribution.

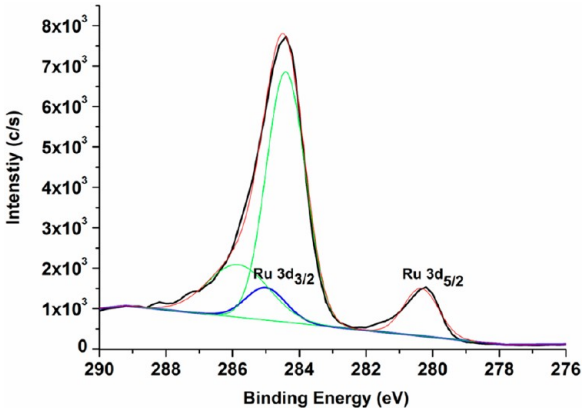

Figure 5. Ru 3d XPS spectrum of Ru(0)@MWCNT with a 1.91 wt % Ru loading.

in the presence of MWCNTs in the temperature range used in this study.

However, Ru(0)@MWCNTs are found to be highly active catalyst in the hydrolysis of ammonia–borane generating 3.0 equivalent H_2 gas per mol of AB in the same temperature range. Expectedly, the catalytic activity depends on the ruthenium loading of catalyst materials. A series of experiments were performed starting with 10 mL solution of 100 mM AB and 0.216 mM Ru using Ru(III)@MWCNT sample with various ruthenium loading (0.73, 1.47, 1.91, 2.26, 2.83 wt % Ru) in appropriate amount to provide the same ruthenium concentration in all of the experiments. The catalytic activity in the hydrolysis of AB at 25.0 ± 0.1 °C shows variation with the ruthenium loading as shown in Figure 6. The Ru(0)@MWCNT sample with ruthenium loading of 1.91 wt % Ru provides the highest catalytic activity in hydrogen generation from the hydrolysis of AB at 25.0 ± 0.1 °C. As the ruthenium loading further increases, the catalytic activity of Ru(0)@MWCNT decreases, most probably due to the agglomeration of nanoparticles, resulting in a decrease in the surface area and the accessibility of active sites.[49] For all the experiments performed in this study, ammonia test was applied following the procedure described elsewhere[33] and no ammonia generation was detected.

Figure 7 shows the plots of equivalent H_2 gas generated per mole of H_3NBH_3 versus time during the catalytic hydrolysis of 100 mM AB solution using Ru(0)MWCNT with a loading of

dx.doi.org/10.1021/am3019146 | ACS Appl. Mater. Interfaces 2012, 4, 6302–6310

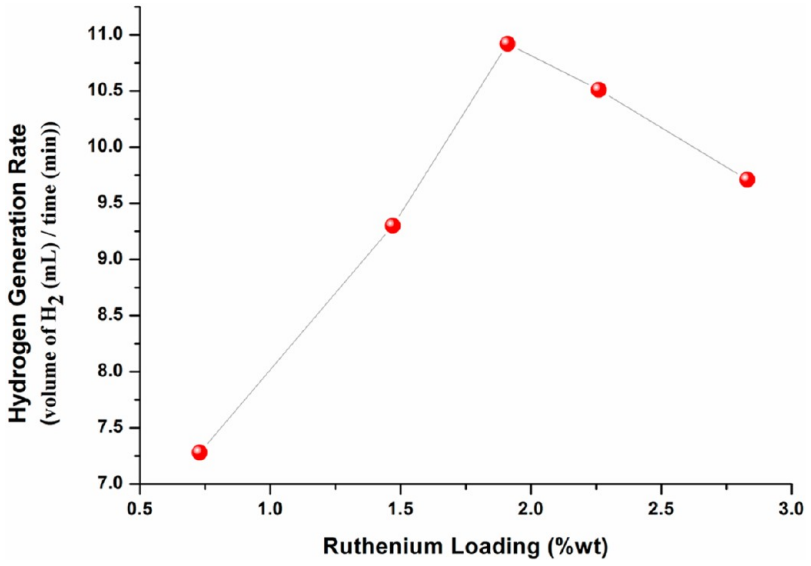

Figure 6. Rate of hydrogen generation versus Ru loading in weight percentage for the hydrolysis of AB (100 mM) catalyzed by Ru(0)@MWCNT with various Ru loading (0.216 mM Ru) at 25.0 ± 0.1 °C.

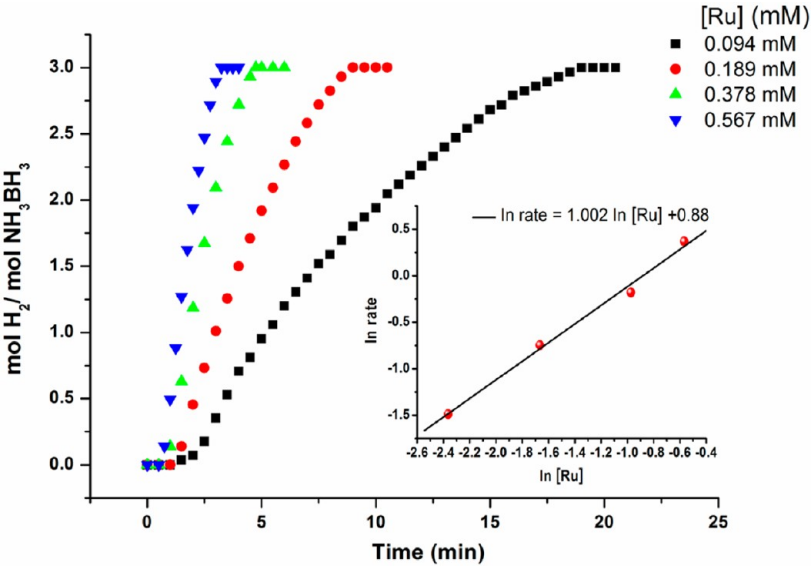

Figure 7. mol H_2/mol H_3NBH_3 versus time graph depending on the ruthenium concentration in Ru(0)MWCNT for the hydrolysis of AB (100 mM) at 25.0 ± 0.1 °C. The inset shows the plot of hydrogen generation rate versus the concentration of Ru, both in logarithmic scale.

1.91 wt % Ru as catalyst in different ruthenium concentration at 25.0 ± 0.1 °C. The hydrogen generation rate was determined from the linear portion of each plot. For all the tests a complete hydrogen release (mol H_2/mol H_3NBH_3 = 3.0) was observed. The inset in Figure 7 shows the plot of hydrogen generation rate versus initial concentration of ruthenium, both in logarithmic scale, which gives a straight line with a slope of 1.0 indicating that hydrolysis of AB is first-order with respect to the ruthenium concentration.

The turnover frequency for hydrogen generation from the hydrolysis of AB (100 mM) at 25.0 ± 0.1 °C was determined to be TOF = 329 min^{-1} (mol H_2/mol Ru min) from the hydrogen generation rate in the linear portion of plots given in Figure 7 for experiments starting with 100 mM AB plus Ru(III)-MWCNT with a loading of 1.91 wt % Ru in different ruthenium concentration. It is worth noting that Ru(0)@MWCNTs provide the highest TOF value ever reported for the hydrolysis of ammonia−borane using ruthenium catalysts such as Laurate-stabilized Ru(0) nanoclusters (TOF = 75 min^{-1}),[50] PSSA-co-MA stabilized Ru(0) nanoclusters (TOF = 172 min^{-1}),[51] Ru@Al_2O_3 (TOF = 83.3 min^{-1}),[52] Ru/Carbon (TOF = 113 min^{-1}).[19] The catalytic activity of Ru(0)@MWCNTs is even higher than that of zeolite framework stabilized rhodium(0) nanocluster (TOF = 92 min^{-1}),[22] but lower than that of colloidal Rh(0) (TOF = 900 min^{-1}).[21] The high catalytic activity of Ru(0)@MWCNTs can be attributed to the good dispersion of nanoparticles on the surface of carbon nanotubes. The contact area between the nanoparticles and the support is small, so that the active sites on the surface of nanoparticles are accessible.

The catalytic hydrolysis of ammonia−borane was carried out at various temperature in the range of 20−40 °C starting with Ru(III)@MWCNT (loading = 1.91 wt % Ru and [Ru] = 0.189 mM) plus 100 mM AB in 10 mL of water. The rate constants

dx.doi.org/10.1021/am3019146 | ACS Appl. Mater. Interfaces 2012, 4, 6302−6310

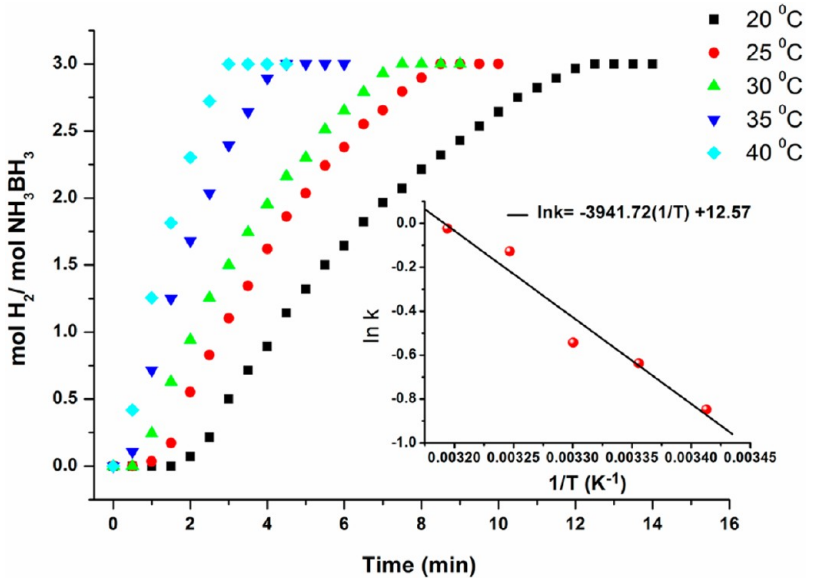

Figure 8. mol H_2 /mol H_3NBH_3 versus time graph for the hydrolysis of AB (100 mM) using Ru(0)@MWCNT ([Ru] = 0.189 mM) as catalyst at different temperatures. The inset shows the Arrhenius plot.

for the hydrogen generation at different temperature were calculated from the slope of linear part of each plot given in Figure 8 and used for the calculation of activation energy (E_a = 33 ± 2 kJ/mol) from the Arrhenius plot, which is shown in the inset of Figure 8. Ru(0)@MWCNTs provide lower activation energy than most of the catalyst reported in the literature for the same reaction using ruthenium: 47 kJ/mol for Laurate-stabilized Ru(0) nanoclusters,[50] 54 kJ/mol for PSSA-co-MA stabilized Ru(0) nanoclusters,[51] 48 kJ/mol for Ru@Al_2O_3,[52] 76 kJ/mol for Ru/Carbon.[19] However, the activation energy (23 kJ/mol) of Ru/γ-Al_2O_3 is lower than that of Ru(0)@MWCNTs for reasons described elsewhere.[18,50] The low activation energy observed for the hydrolysis of AB catalyzed by Ru(0)@MWCNTs reflects the role of carbon nanotubes as support for the nanoparticles. Nanoparticles on the surface of carbon nanotubes can freely bind the substrate and provide a reduction of bond strength, which will be broken in the catalytic cycle.

Reusability test of Ru(0)@MWCNTs was performed using the catalyst isolated from the reaction solution after a previous run of hydrolysis of AB. After the completion of hydrogen generation from the hydrolysis of AB starting with 0.567 mM Ru(III)@MWCNT plus 100 mM AB in 10 mL aqueous solution at 25.0 ± 0.1 °C, the catalyst was isolated by filtering and washing with water and dried in the oven at 120 °C. The whole powder materials were weighed and then redispersed in 10 mL of solution containing 100 mM AB and a second run hydrolysis was started immediately and continued until the completion of hydrogen evolution. This was repeated four times. Figure 9 shows the percentage of initial catalytic activity of Ru(0)@MWCNTs in the subsequent catalytic hydrolysis of 100 mM ammonia–borane performed by using the catalyst isolated after the previous run of hydrolysis at 25.0 ± 0.1 °C. The reusability tests reveal that Ru(0)@MWCNTs are still active in the subsequent runs of hydrolysis of ammonia–borane providing a release of 3.0 equivalent H_2 per mole of NH_3BH_3. After the fourth run hydrolysis of ammonia–borane, Ru(0)@MWCNTs preserve 41% of their initial catalytic activity. TEM images of Ru(0)@MWCNT after the forth reuse in the hydrolysis of ammonia–borane (see Figure S1 in the

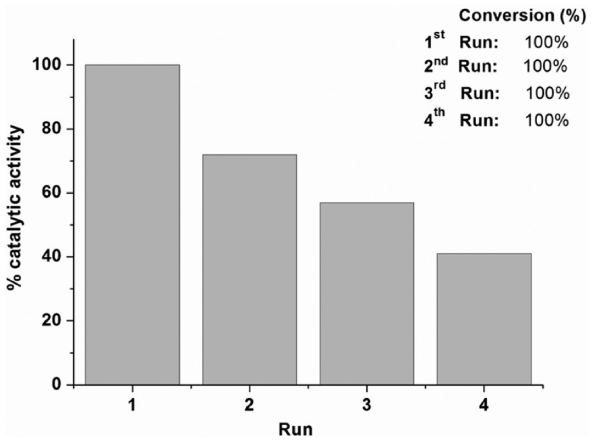

Figure 9. Percentage of initial catalytic activity of Ru(0)@MWCNT ([Ru] = 0.567 mM) in successive runs after the reuse for the hydrolysis of ammonia–borane (100 mM).

Supporting Information) show that ruthenium(0) nanoparticles aggregate on MWCNT after the forth reuse. The aggregation of metal nanoparticles causes a decrease in the surface area of nanoparticles. Therefore, the decrease in catalytic activity in successive runs can be attributed to the agglomeration of nanoparticles on the surface of carbon nanotubes during the isolation and redispersion processes, as the material loss has already been taken into account in calculating the activity in each run.

Catalytic lifetime of Ru(0)@MWCNTs was measured by the total turnover number (TTO) in the hydrolysis of ammonia–borane. A catalyst lifetime experiment starting with 1.89 μmol Ru in 100 mL of solution of AB at 25.0 ± 0.1 °C reveals a minimum TTO value of 26400 turnovers over 29 h in the hydrolysis of AB before deactivation of the catalyst. An initial TOF value of 329 min^{-1} was obtained; however, the average TOF value was calculated to be 15 min^{-1} in the catalytic lifetime experiment. The observation that the TOF value decreases as the reaction proceeds indicates the deactivation of ruthenium(0) nanoparticles catalyst. After the lifetime experi-

dx.doi.org/10.1021/am3019146 | ACS Appl. Mater. Interfaces 2012, 4, 6302–6310

ment, the resulting solution was filtered and the ruthenium concentration of filtrate was found to be 0.085 ppm as determined by ICP-OES. This indicates that 96% of ruthenium nanoparticles still remain on the surface of carbon nanotubes after lifetime experiment. Therefore, the deactivation of Ru(0)@MWCNTs catalyst can be attributed to a decrease in accessibility of active sites of ruthenium nanoparticles due the passivation of metal surface by metaborate ions which accumulate in solution as the reaction proceeds.[32]

CONCLUSIONS

In summary, ruthenium(0) nanoparticles supported on multiwalled carbon nanotube catalyst (Ru(0)@MWCNT) were easily generated in situ during the hydrolysis of ammonia borane and they showed remarkably high catalytic activity with an initial turn over frequency of 329 min^{-1} at room temperature. Ru(0)@MWCNT is found to be an outstanding catalyst for the hydrolysis of AB with the highest TOF value among all reported ruthenium catalysts. The reusability and lifetime experiments show that Ru(0)@MWCNTs are still active catalyst in the hydrolysis of ammonia−borane even after the fourth run preserving 41% of their initial catalytic activity and also providing 26400 turnovers over 29 h in the hydrolysis of AB at 25.0 ± 0.1 °C before deactivation. Activation energy for the hydrolysis of AB in the presence of Ru(0)@MWCNT was determined as 33 ± 2 kJ/mol from the evaluation of kinetic data at various temperatures. Ru(0)@MWCNTs provide lower activation energy than most of the catalyst reported in the literature for the same reaction using ruthenium. Easy preparation and the high catalytic performance of Ru(0)@MWCNT reveal that ruthenium(0) nanoparticle catalyst supported on multiwalled carbon nanotubes is a promising candidate to be employed in developing highly efficient, portable hydrogen generation systems using AB.

ASSOCIATED CONTENT

Supporting Information

Figure S1, TEM images of Ru(0)@MWCNT with a 1.91 wt % Ru loading after the forth reuse in the hydrolysis of ammonia−borane. This material is available free of charge via the Internet at http://pubs.acs.org/.

AUTHOR INFORMATION

Corresponding Author

*Tel: +90 312 210 3212. Fax: +90 312 210 3200. E-mail: sozkar@metu.edu.tr.

Notes

The authors declare no competing financial interest.

ACKNOWLEDGMENTS

We gratefully acknowledged the partial support from Turkish Academy of Sciences and the Scientific and Technological Research Council of Turkey (a fellowship for S.A. within IntenC exchange program between Middle East Technical University and Technische Universität Darmstadt). We thank Prof. Dr. Jörg J. Schneider for lab facilities in Laboratory of Inorganic Chemistry at the Technische Universität Darmstadt. We thank Prof. Dr. Deniz Üner at METU, Department of Chemical Engineering, for helpful discussions and suggestions.

REFERENCES

(1) Schlapbach, L.; Züttel, A. *Nature* **2001**, *414*, 353−358.
(2) Grochala, W.; Edwards, P. P. *Chem. Rev.* **2004**, *104*, 1283−1316.
(3) Chen, P.; Zhu, M. *Mater. Today* **2008**, *11*, 36−43.
(4) Rosi, N. L.; Eckert, J.; Eddaoudi, M.; Vodak, D. T.; Kim, J.; Keefle, M. O.; Yaghi, O. M. *Science* **2003**, *300*, 1127−1129.
(5) Germain, J.; Freechet, J. M.J.; Svec, F. *Small* **2009**, *10*, 1098−1111.
(6) Sandrock, G. *J. Alloys Compd.* **1999**, *293*, 877−888.
(7) Bogdanovic, B.; Schwickardi, M. *J. Alloys Compd.* **1997**, *253*, 1−9.
(8) Chen, P.; Xiong, Z. T.; Luo, J. Z.; Lin, J. Y.; Tan, K. L. *Nature* **2002**, *420*, 302−304.
(9) Staubitz, A.; Robertson, A. P. M.; Manners, I. *Chem. Rev.* **2010**, *110*, 4079−4124.
(10) Marder, T. B. *Angew. Chem., Int. Ed.* **2007**, *46*, 8116−8118.
(11) Ramachandran, P. V.; Gagare, P. D. *Inorg. Chem.* **2007**, *46*, 7810−7817.
(12) Ramzan, M.; Silvearv, F.; Blomqvist, A.; Scheicher, R. H.; Lebeque, S.; Ahuja, R. *Phys. Rev. B* **2009**, *79*, 132102−4.
(13) Xu, Q.; Chandra, M. *J. Power Sources* **2006**, *163*, 364−370.
(14) Wolf, G.; Baumann, J.; Baitalow, J.; Hoffmann, F. P. *Thermochim. Acta* **2000**, *343*, 19−25.
(15) Erdogan, H.; Metin, Ö.; Özkar, S. *Phys. Chem. Chem. Phys.* **2009**, *11*, 10519−10525.
(16) Erdogan, H.; Metin, Ö.; Özkar, S. *Catal. Today* **2011**, *170*, 93−98.
(17) Çalışkan, S.; Zahmakıran, M.; Özkar, S. *Appl. Catal., B* **2010**, *93*, 387−394.
(18) Chandra, M.; Xu, Q. *J. Power Sources* **2007**, *168*, 135−142.
(19) Basu, S.; Brockman, A.; Gagare, P.; Zheng, Y.; Ramachandran, P. V.; Delgass, W. N.; Gore, J. P. *J. Power Sources* **2009**, *188*, 238−243.
(20) Rachiero, G. P.; Demirci, U. B.; Miele, P. *Catal. Today* **2011**, *170*, 85−92.
(21) Clark, T. J.; Whittell, G. R.; Manners, I. *Inorg. Chem.* **2007**, *46*, 7522−7527.
(22) Zahmakıran, M.; Özkar, S. *Appl. Catal., B* **2009**, *89*, 104−110.
(23) Durap, F.; Zahmakıran, M.; Özkar, S. *Appl. Catal., A* **2009**, *369*, 53−59.
(24) Rakap, M.; Özkar, S. *Int. J. Hydrogen Energy* **2010**, *35*, 1305−1312.
(25) Rakap, M.; Özkar, S. *Int. J. Hydrogen Energy* **2011**, *36*, 7019−7027.
(26) Yan, J.; Zhang, X.; Han, S.; Shioyama, H.; Xu, Q. *Angew. Chem., Int. Ed.* **2008**, *47*, 2287−2289.
(27) Umegaki, T.; Yan, J.-M.; Zhang, X.-B.; Shioyama, H.; Kuriyama, N.; Xu, Q. *J. Power Sources* **2010**, *195*, 8209−8214.
(28) Patel, N.; Fernandes, R.; Guella, G.; Miotello, A. *Appl. Catal., B* **2010**, *95*, 137−143.
(29) Rakap, M.; Özkar, S. *Int. J. Hydrogen Energy* **2010**, *35*, 3341−3346.
(30) Song, Li, Y.; Li, W.; He, B.; Yang, J.; Li, X. *Int. J. Hydrogen Energy* **2011**, *36*, 10468−10473.
(31) Metin, Ö.; Dinç, M.; Eren, Z. S.; Özkar, S. *Int. J. Hydrogen Energy* **2011**, *36*, 11528−11535.
(32) Zahmakıran, M.; Ayvalı, T.; Akbayrak, S.; Çalışkan, S.; Çelik, D.; Özkar, S. *Catal. Today* **2011**, *170*, 76−84.
(33) Metin, Ö.; Özkar, S. *Int. J. Hydrogen Energy* **2011**, *36*, 1424−1432.
(34) Özkar, S.; Finke, R. G. *J. Am. Chem. Soc.* **2002**, *124*, 5796−5810.
(35) Özkar, S.; Finke, R. G. *Langmuir* **2002**, *18*, 7653−7662.
(36) Planeix, J. M.; Coustel, N.; Coq, B.; Brotons, V.; Kumbhar, P. S.; Dutartre, R.; Geneste, P.; Bernier, P.; Ajayan, P. M. *J. Am. Chem. Soc.* **1994**, *116*, 7935−7936.
(37) Jinshan, L. *Carbon* **2007**, *45*, 1599−1605.
(38) Yin, S.-F.; Xu, B.-Q.; Ng, C.-F.; Au, C.-T. *Appl. Catal., B* **2004**, *48*, 237−241.
(39) Yang, X.; Wang, X.; Qiu. *J. App. Catal., A* **2010**, *382*, 131−137.
(40) Deng, W.; Liu, M.; Tan, X.; Zhang, Q.; Wang, Y. *J. Catal.* **2010**, *271*, 22−32.
(41) Sun, Z.; Liu, Z.; Han, B.; Wang, Y.; Du, J.; Xie, Z.; Han, G. *Adv. Mater.* **2005**, *17*, 928−832.

(42) Watzky, M. A.; Finke, R. G. *J. Am. Chem. Soc.* **1997**, *119*, 10382−10400.
(43) Widegren, J. A.; Aiken, J. D.; Özkar, S.; Finke, R. G. *Chem. Mater.* **2001**, *13*, 312−324.
(44) Widegren, J. A.; Bennett, M. A.; Finke, R. G. *J. Am. Chem. Soc.* **2003**, *125*, 10301−10310.
(45) Jin, C.; Xia, W.; Nagaiah, T. C.; Guo, J.; Chen, X.; Bron, M.; Schuhmann, W.; Muhler, M. *Electrochim. Acta* **2009**, *54*, 7186−7193.
(46) Sun, Z.; Zhang, X.; Na, N.; Liu, Z.; Han, B.; An, G. *J. Phys. Chem. B* **2006**, *110*, 13410−13414.
(47) Zhang, H.; Chu, W.; Zou, C.; Huang, Z.; Ye, Z.; Zhu, L. *Catal. Lett.* **2010**, *141*, 438−444.
(48) Wagner, C.; Muilenber, G. E.; Riggs, W. M.; Davis, L. E.; Moulder, J. F. *Handbook of X-ray Photoelectron Spectroscopy*; Physical Electronic Division, Perkin-Elmer: Eden Prairie, MN, 1979; Vol. 55.
(49) López, E.; Kim, J.; Shanmugharaj, A. M.; Ryu, S. H. *J. Mater. Sci.* **2012**, *47*, 2985−2994.
(50) Durap, F.; Zahmakıran, M.; Özkar, S. *Int. J. Hydrogen Energy* **2009**, *34*, 7223−7230.
(51) Metin, Ö.; Şahin, Ş.; Özkar, S. *Int. J. Hydrogen Energy* **2009**, *34*, 6304−6313.
(52) Can, H.; Metin, Ö. *Appl. Catal., B* **2012**, *125*, 304−310.